Inorganic Chemistry
Article

Inorg. Chem. **2010**, *49*, 5853–5858 **5853**
DOI: 10.1021/ic902559n

A Five-Coordinate [2Fe−2S] Cluster

Michael G. G. Fuchs, Sebastian Dechert, Serhiy Demeshko, Ulf Ryde, and Franc Meyer*

Institut für Anorganische Chemie, Georg-August-Universität, Tammannstrasse 4, 37077 Göttingen, Germany, and Department of Theoretical Chemistry, Lund University, Chemical Centre, P.O. Box 124, 221 00 Lund, Sweden

Received December 22, 2009

A unique [2Fe−2S] cluster (**1**) with genuinely five-coordinate ferric ions has been synthesized and investigated both structurally and spectroscopically. The crystal structure of **1** as well as ^{1}H NMR data reveal that 2,6-bis(imidazol-2-yl)pyridine binds to the [2Fe−2S] core as a tridentate capping ligand. DFT calculations showing spin density on all coordinating atoms support this finding. Cluster **1** has also been characterized by Mössbauer and UV/vis spectroscopy, mass spectrometry, cyclic voltammetry, and magnetic susceptibility measurements. Significant spectroscopic properties that make **1** distinct from conventional [2Fe−2S] clusters include a rather small quadrupole splitting of 0.43 mm/s.

Introduction

The coordination geometry of the metal ions in the vast majority of biological Fe/S clusters is distorted tetrahedral.[1−3] This situation is also found in various biomimetic complexes, where many of the structural and electronic properties of the natural systems have been reproduced.[2] Yet, the protein environment has more means to influence cluster properties than most of the small ligands hitherto used in synthetic coordination compounds, and some essential properties of naturally occurring Fe/S clusters (such as the redox potentials of [2Fe−2S] ferredoxins) have not been fully emulated yet.

Although reduction potentials and other properties of biomimetic [2Fe−2S] clusters can be tuned to a certain extent by variation of the ligand substitution,[4] these influences are not sufficient to accomplish the versatility exhibited by natural clusters. Probably the most prominent example is the exceptionally positive redox potential displayed by some Rieske-type [2Fe−2S] clusters coordinated by two cysteines and two histidines; even though a structural analogue has recently been reported, the most important feature—the redox potential—is not comparable to that of the natural archetype.[5] Apart from the Rieske-type clusters bearing histidine ligands, it is mainly the [2Fe−2S] cluster in biotin synthase that has a distinct ligand sphere. One of the ligands is an arginine residue,[6] which is very unusual for biological metal ligation.[7] The low resolution of the crystal structure does not allow for definite assignment of the protonation state and the coordination mode of this arginine residue, but unusual interactions are conceivable, including bidentate arginine coordination and the involvement in various hydrogen bonds.

Coordination numbers greater than four have been observed at individual iron atoms in some [4Fe−4S] proteins,[6,8−12] and this was successfully emulated in some site-differentiated synthetic [4Fe−4S] clusters.[13,14] However, interactions other than via the four terminal ligands have been explored only scarcely in synthetic [2Fe−2S] clusters, namely, hydrogen bonding[15] and weak coordination by an additional donor atom.[16] The latter concept of secondary bonding interactions, inspired particularly by the potentially bidentate coordination of arginine in biotin synthase,[17] is here extended toward [2Fe−2S] clusters containing iron atoms with a genuine coordination number of five.

*To whom correspondence should be addressed. E-mail: franc.meyer@chemie.uni-goettingen.de.

(1) Beinert, H.; Holm, R. H.; Münck, E. *Science* **1997**, *277*, 653–659.
(2) Rao, P. V.; Holm, R. H. *Chem. Rev.* **2004**, *104*, 527–559.
(3) Meyer, J. *J. Biol. Inorg. Chem.* **2008**, *13*, 157–170.
(4) Ballmann, J.; Dechert, S.; Demeshko, S.; Meyer, F. *Eur. J. Inorg. Chem.* **2009**, 3219–3225.
(5) Ballmann, J.; Albers, A.; Demeshko, S.; Dechert, S.; Bill, E.; Bothe, E.; Ryde, U.; Meyer, F. *Angew. Chem.* **2008**, *120*, 9680–9684.
(6) Berkovitch, F.; Nicolet, Y.; Wan, J. T.; Jarrett, J. T.; Drennan, C. L. *Science* **2004**, *303*, 76–79.
(7) Di Costanzo, L.; Flores, L. V., Jr.; Christianson, D. W. *Proteins* **2006**, *65*, 637–642.
(8) Lauble, H.; Kennedy, M. C.; Beinert, H.; Stout, C. D. *J. Mol. Biol.* **1994**, *237*, 437–451.
(9) Layer, G.; Moser, J.; Heinz, D. W.; Jahn, D.; Schubert, W.-D. *EMBO J.* **2003**, *22*, 6214–6224.
(10) Dai, S.; Friemann, R.; Glauser, D. A.; Bourquin, F.; Manieri, W.; Schürmann, P.; Eklund, H. *Nature* **2007**, *448*, 92–98.
(11) Hänzelmann, P.; Schindelin, H. *Proc. Natl. Acad. Sci. U. S. A.* **2004**, *101*, 12870–12875.
(12) Lepore, B. W.; Ruzicka, F. J.; Frey, P. A.; Ringe, D. *Proc. Natl. Acad. Sci. U. S. A.* **2005**, *102*, 13819–13824.
(13) Zhou, C.; Holm, R. H. *Inorg. Chem.* **1997**, *36*, 4066–4077.
(14) van Strijdonck, G. P. F.; ten Have, P. T. J. H.; Feiters, M. C.; van der Linden, J. G. M.; Steggerda, J. J.; Nolte, R. J. M. *Chem. Ber.* **1997**, *130*, 1151–1157.
(15) Ueyama, N.; Yamada, Y.; Okamura, T.; Kimura, S.; Nakamura, A. *Inorg. Chem.* **1996**, *35*, 6473–6484.
(16) Ballmann, J.; Dechert, S.; Bill, E.; Ryde, U.; Meyer, F. *Inorg. Chem.* **2008**, *47*, 1586–1596.
(17) Fuchs, M. G. G.; Meyer, F.; Ryde, U. *J. Biol. Inorg. Chem.* **2010**, *15*, 203–212.

Published on Web 06/02/2010

Scheme 1. Synthesis of Complex **1**

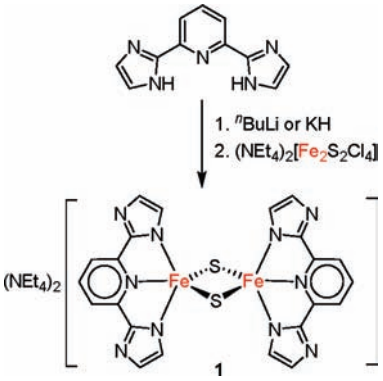

A suitable tridentate capping ligand for the [2Fe−2S] core should be diprotic (since synthetic [2Fe−2S] clusters in their diferric state are usually stabilized by two anionic terminal ligands) and should provide a preorganized pocket with three donor atoms that can bind equally. 2,6-Bis(imidazol-2-yl)-pyridine[18] (H_2L) was thus chosen as a promising ligand. As H_2L has been shown to give iron complexes whose reduction potential can be tuned by protonation of the noncoordinating N atoms,[19] the potential for investigating proton-coupled electron transfer reactions as observed in Rieske proteins was an additional incentive for the choice of this particular ligand scaffold.

Results and Discussion

When H_2L was treated with ^{n}BuLi or KH in DMF and $(NEt_4)_2[Fe_2S_2Cl_4]$[20] was subsequently added, the deep red color typical for [2Fe−2S] clusters was retained. Slow diffusion of Et_2O into a complex solution caused precipitation of a powder that showed the expected signals in the ^{1}H NMR spectrum. In addition, crystals suitable for X-ray diffraction were obtained, and the product could be identified as the target complex **1**. Due to gradual decomposition in DMF (and moreso in DMSO), no pure bulk material could be obtained by recrystallization from DMF/Et_2O. However, when the synthesis was performed in THF/MeCN, **1** precipitated within a few hours and could be collected by filtration (Scheme 1); this material proved to be pure according to NMR and Mössbauer spectroscopy. The main challenge in the synthesis is to avoid cluster degradation and formation of the undesired $[L_2Fe^{II}]^{2-}$ or $[L_2Fe^{III}]^{-}$ species (usually observed as major products with many related ligands), which requires optimization and meticulous control of the reaction conditions. Complex **1** is only sparingly soluble but stable in MeCN, while it decomposes in DMF and DMSO solutions.

The crystal structure of **1** shows an intact sulfide-bridged diferric cluster core coordinated by two tridentate capping ligands (Figure 1). Although the distances between the iron atoms and the imidazole N atoms are shorter (2.11 and 2.12 Å), the pyridine N atoms are clearly within bonding distance (2.18 Å). Compared to most other [2Fe−2S] clusters, the Fe···Fe distance in **1** is somewhat elongated to 2.79 Å but is

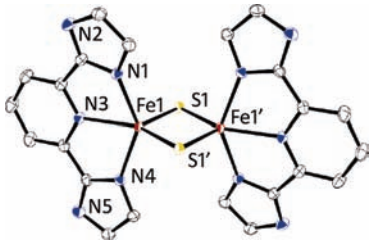

Figure 1. Molecular structure of **1**. ORTEP plot, with 50% probability thermal ellipsoids. Counterions and hydrogen atoms are omitted for clarity; only crystallographically independent heteroatoms are labeled. Symmetry operation used to generate equivalent atoms: (′) $1-x$, $1-y$, $1-z$.

in the range previously observed for clusters with secondary bonding interactions (cf. 2.80 Å in a cluster bearing potentially tridentate capping ligands that exhibit weak thioether coordination with d(Fe···S) = 2.78/2.91 Å in addition to the binding of two thiolates[16]). This goes along with an increase of the Fe−S−Fe angle to 77.7° compared to 74−76° for normal [2Fe−2S] clusters with four-coordinate metal ions.[2] The angle N1−Fe1−N4 in **1** (141.3°) deviates significantly from 180°, and the coordination geometry of the ferric ions is best described as square pyramidal with one of the bridging sulfide ions occupying the apical position. Accordingly, the τ_5 value, which quantifies the degree of trigonality,[21] is close to zero (0.085). The Fe1−S1 bond involving the apical S atom (2.24 Å) is slightly longer than Fe1−S1′ in the basal plane (2.21 Å). All relevant distances and angles are collected in Table 1.

The ^{1}H NMR spectrum of **1** in DMF-d_7 shows typically broad signals at 12.83 and 13.71 ppm for the imidazole protons and at 6.90 and 9.00 ppm for the pyridine protons (Figure 2). The pronounced broadening of the latter signal is further proof for genuine coordination by the pyridine moiety. The two imidazole signals appear at a remarkably low field compared to ligand signals in other N-coordinate [2Fe−2S] clusters.[22]

The UV/vis spectrum of **1** resembles that of more conventional [2Fe−2S] clusters (Figure 3). Besides an intense band at 310 nm with a shoulder at 370 nm, there is a band with much lower intensity in the visible region at 489 nm, presumably a charge-transfer absorption. Compared to clusters with tetrahedral metal ions bearing bidentate N-donor capping ligands,[22] both bands are shifted to higher energies.

Electrochemical investigations on **1** are hampered by its low stability in DMF or DMSO and poor solubility in other solvents. Cyclic voltammetry (CV) of a DMF solution reveals that **1** is irreversibly reduced at rather low potentials (cathodic peak potential $E_p^c = -1.37$ V vs the $Cp^*_2Fe/Cp^*_2Fe^+$ couple or −1.14 V vs NHE;[23] at 100 mV/s in 0.1 M DMF/$N^nBu_4PF_6$). Over time, however, a reversible redox wave at $E_{1/2} = -0.75$ V vs $Cp^*_2Fe/Cp^*_2Fe^+$ (−0.52 V vs NHE) gradually develops at the expense of the response for **1** (see the Supporting Information). This can be assigned to the $[L_2Fe^{III}]^-/[L_2Fe^{II}]^{2-}$ couple,[19] indicating cluster decomposition under the conditions of the CV experiment.

(18) Stupka, G.; Gremaud, L.; Bernardinelli, G.; Williams, A. F. *Dalton Trans.* **2004**, 407–412.
(19) Carina, R. F.; Verzegnassi, L.; Bernardinelli, G.; Williams, A. F. *Chem. Commun.* **1998**, 2681–2682.
(20) Do, Y.; Simhon, E. D.; Holm, R. H. *Inorg. Chem.* **1983**, *22*, 3809–3812.
(21) Addison, A. W.; Rao, T. N.; Reedijk, J.; van Rijn, J.; Verschoor, G. C. *J. Chem. Soc., Dalton Trans.* **1984**, 1349–1356.
(22) Ballmann, J.; Sun, X.; Dechert, S.; Bill, E.; Meyer, F. *J. Inorg. Biochem.* **2007**, *101*, 305–312.
(23) Aranzaes, J. R.; Daniel, M.-C.; Astruc, D. *Can. J. Chem.* **2006**, *84*, 288–299.

Table 1. Selected Interatomic Distances and Angles of **1**

	d(Fe···Fe)/Å	d(Fe−μ-S)/Å	d(Fe−$N_{imidazole}$)/Å	d(Fe−$N_{pyridine}$)/Å	α(Fe−μ-S−Fe)/deg	α($N_{imidazole}$−Fe−$N_{imidazole}$)/deg	α(Fe···Fe−$N_{pyridine}$)/deg	τ_5[a]
experimental	2.7911(3)	2.2136(4) 2.2377(4)	2.1139(16) 2.1177(13)	2.1799(12)	77.660(14)	141.300(56)	162.81(3)	0.085
calculated (BP86)	2.78	2.24 2.22	2.16	2.22	77.2	140.3	161.3	0.12
calculated (B3LYP)	2.92	2.28 2.27	2.17	2.24	79.9	139.6	161.6	0.15

[a] Calculated according to $\tau_5 = (\beta - \alpha)/60°$ with α and β being the two largest bond angles.[21]

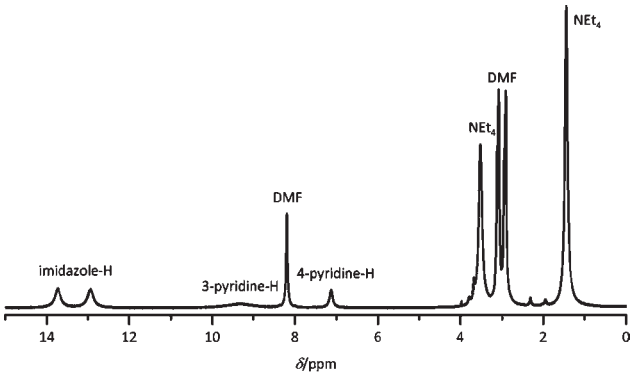

Figure 2. ^{1}H NMR spectrum of **1** recorded at 500 MHz in DMF-d_7.

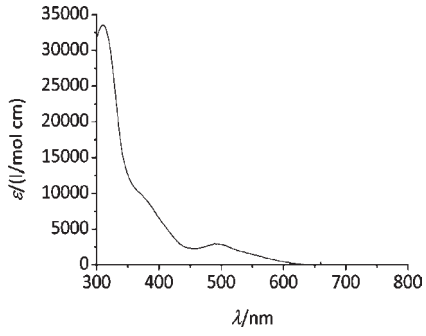

Figure 3. UV/vis spectrum of cluster **1** in DMSO.

The Mössbauer spectrum of **1** (Figure 4) shows a single quadrupole doublet with isomer shift $\delta = 0.44$ mm/s, which is rather positive compared to other N-coordinate [2Fe−2S] clusters; e.g., a cluster with a methylindolate capping ligand shows $\delta = 0.29$ mm/s.[24] While a linear correlation between the oxidation state s of the iron atoms and the isomer shift according to $\delta = 1.4-0.4\,s$ was reported in the literature, this calculation holds only for tetrahedral sites and thus cannot be applied to the present system with five-coordinate iron atoms.[25] However, a shift to larger δ values is known from site-differentiated [4Fe−4S] clusters with coordination numbers greater than four for one of the iron atoms.[2,26] While this has been qualitatively explained by the decrease in spectroscopic oxidation number that results from the electron density provided by the additional donor atom, no quantitative correlation has yet been found.

Furthermore, a surprisingly small quadrupole splitting was observed for **1** ($\Delta E_Q = 0.43$ mm/s). This value was compared

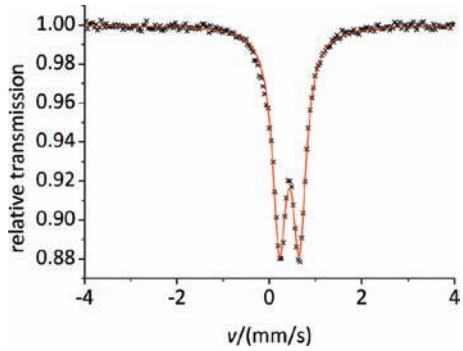

Figure 4. Mössbauer spectrum of **1** at 80 K.

to theoretical quadrupole splittings obtained by DFT calculations using two different functionals, namely, BP86[27,28] and B3LYP.[29,30] Calculations using crystal coordinates gave lower values than those using the optimized geometry (Table 2), which for both BP86 and B3LYP agrees quite well with the geometry determined by X-ray diffraction (Table 1). In all cases, a relatively small value was obtained (BP86, 0.18/0.17 (crystal coordinates) and 0.30 mm/s (optimized coordinates); B3LYP, 0.13/0.15 and 0.22 mm/s, respectively); the method without exact exchange (BP86) was closer to the value found experimentally. Although the calculated values are not very exact, the overall trend is correctly reproduced. Like in similar cases,[5,24] calculated values are smaller than experimental values, which therefore seems to be a general trend for [2Fe−2S] clusters when using this DFT method. Compared to other N-coordinated [2Fe−2S] clusters for which quadrupole splittings have been calculated at the BP86 level of theory,[5] both the experimental and the calculated value is smallest in the case of **1**.

Magnetic susceptibility measurements were performed at 0.5 T from 295 to 2 K (see the Supporting Information for details). As for other [2Fe−2S] clusters, the magnetic moment μ_{eff} decreases upon cooling, indicating a diamagnetic ground state ($S_T = 0$) with strongly antiferromagnetically coupled ferric ions. The coupling ($J = -167$ cm^{-1}) is in the same range as the coupling determined for clusters with bidentate dipyrromethane ligands.[22] However, the coupling is much stronger than in a cluster with a dithiolate ligand that imposes additional secondary bonding interaction via a chelating thioether group ($J = -126$ cm^{-1}).[16] Since the relevant distances and angles within the cluster core of the two complexes are very similar (d(Fe···Fe) = 2.79 Å as compared to 2.80 Å, α(Fe−μ-S−Fe) = 77.66° as compared to 78.06/78.45°), the

(24) Fuchs, M. G. G.; Dechert, S.; Demeshko, S.; Meyer, F. *Eur. J. Inorg. Chem.* **2010**, DOI: 10.1002/ejic.201000418.
(25) Hoggins, J. T.; Steinfink, H. *Inorg. Chem.* **1976**, *15*, 1682–1685.
(26) Ciurli, S.; Carrié, M.; Weigel, J. A.; Carney, M. J.; Stack, T. D. P.; Papaefthymiou, G. C.; Holm, R. H. *J. Am. Chem. Soc.* **1990**, *112*, 2654–2664.
(27) Perdew, J. P. *Phys. Rev. B* **1986**, *33*, 8822–8824.
(28) Becke, A. D. *Phys. Rev. A* **1988**, *38*, 3098–3100.
(29) Becke, A. D. *J. Chem. Phys.* **1993**, *98*, 5648–5652.
(30) Stephens, P. J.; Devlin, F. J.; Frisch, M. J.; Chabalowski, C. F. *J. Phys. Chem.* **1994**, *98*, 11623–11627.

Table 2. Selected Electrochemical and Spectroscopic Data of Complex **1**

λ_{max}/nm	ε/(l/(mol·cm))	E^c_p[a]/V	δ/(mm/s)	ΔE_Q/(mm/s)	ΔE_Q(calc.)[b]/(mm/s)	ΔE_Q(calc.)[c]/(mm/s)
310, 370, 489	34000, 10000 (sh), 3000	−1.14	0.44	0.43	0.18/0.17 (BP86) 0.13/0.15 (B3LYP)	0.30 (BP86) 0.22 (B3LYP)

[a] Reduction potentials were measured vs the $Cp^*_2Fe/Cp^*_2Fe^+$ couple and referenced vs NHE.[23] [b] Calculated quadrupole splittings were obtained from the eigenvalues of the electric field gradient at the positions of the iron atoms using crystal coordinates. [c] Calculated quadrupole splittings were obtained from the eigenvalues of the electric field gradient at the positions of the iron atoms for an optimized geometry.

Table 3. Calculated Spin Densities on Relevant Atoms of **1**[a]

				ρ/a.u.			
	functional	coupling	$E_{relative}$[b]/(kJ/mol)	Fe	S	$N_{pyridine}$	$N_{imidazole}$
			crystal coordinates				
1	BP86	F	+106	3.91	0.76	0.05	0.07
		AF	0	3.62	0.04	0.05	0.05
	B3LYP	F	+63	4.02	0.72	0.04	0.07
		AF	0	3.94	0.03	0.05	0.06
			optimized coordinates				
1	BP86	F	+81	3.97	0.75	0.04	0.06
		AF	0	3.66	0.03	0.05	0.05
	B3LYP	F	+40	4.06	0.71	0.04	0.06
		AF	0	4.00	0.03	0.04	0.06
$\mathbf{1}^{reduced}$	BP86	F	+25	3.78	0.53	0.03	0.04
		AF	0	3.72/-3.50	0.18/0.22	0.03	−0.03/0.04
	B3LYP	F	+5	3.89	0.48	0.02	0.03
		AF	0	−3.77/3.97	0.39/0.30	0.02	0.02/0.04

[a] Spins are calculated at two levels of theory (BP86 and B3LYP) for the ferromagnetic (F) or antiferromagnetic (AF) states. The oxidized state was considered for crystal and optimized coordinates, the reduced state only for optimized coordinates. When only one value is given, the value on the other respective atom was equal or the negative equivalent; the $N_{imidazole}$ atoms are considered as two pairs of similar atoms. [b] The energy difference between the F and AF states; see the Supporting Information for details.

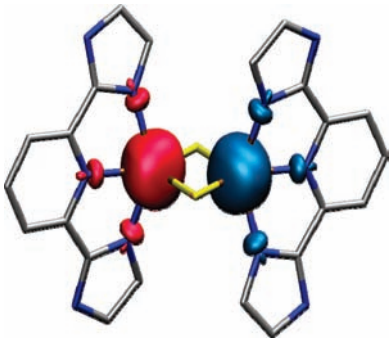

Figure 5. Spin density distribution on **1** (0.01 au contour value; the colors represent α and β spins; results for the AF state, optimized coordinates).

differences in magnetic coupling cannot be explained by the geometry of the [2Fe−2S] cluster core alone. Overall, the magnetic properties of the cluster core of **1** seem to be only slightly perturbed compared to those of related systems with bidentate N-donor capping ligands. The coupling constant has also been calculated on both experimental and optimized geometries using the BP86 and the B3LYP functionals; B3LYP calculations gave better results that match quite well the experimental value (BP86: X-ray coordinates, $J = -341\ cm^{-1}$/optimized coordinates, $-332\ cm^{-1}$; B3LYP: $-208\ cm^{-1}/-154\ cm^{-1}$; see the Supporting Information for details).

In order to quantify the relative spin distribution over the coordinating atoms, spin densities on relevant atoms were calculated in the ferromagnetically and the antiferromagnetically coupled state for both crystal and optimized coordinates. In addition, these calculations were performed also for the reduced (mixed-valent) state with optimized geometry. Relevant values are listed in Table 3. In all cases, the spin density is mainly localized on the iron atoms, and only little spin density is almost equally distributed over the coordinating N atoms, suggesting comparable bond strength (Figure 5).

The energy difference between the antiferromagnetic (AF) and ferromagnetic (F) spin states is large for the oxidized state, favoring the AF state, which is also the one experimentally found. In the reduced state, however, the energy difference becomes smaller. Unfortunately, all attempts to experimentally isolate a reduced mixed-valent species $[\mathbf{1}]^-$ have failed, which in view of the electrochemical findings is no surprise.

Conclusions

Complex **1** reported here is the first synthetic example of a [2Fe−2S] cluster with genuinely five-coordinate iron atoms. This leads to a slight increase in the Fe···Fe distance and Fe−S−Fe angles compared to conventional ferredoxin models. The Mössbauer parameters are also perturbed: the isomer shift is more positive than that of related four-coordinate [2Fe−2S] clusters, and the quadrupole splitting is unusually small. Spin density is concentrated on the ferric ions, but equal distribution of delocalized spin densities over all coordinating N atoms obtained from DFT calculations supports a true five-coordinate nature of the iron atoms. This is furthermore confirmed by the line broadening of the pyridine signals in the ^{1}H NMR spectrum. An attractive option for future work might be the study of a proton-coupled reduction of **1**, because of the presence of noncoordinating and

protonable N atoms in the ligand backbone; this situation bears some resemblance to the histidine-ligated site of Rieske-type [2Fe−2S] clusters. Unfortunately, however, the limited stability of **1** in solution has hindered further investigations so far.

While such systems have not yet been discovered in nature, complex **1** provides valuable benchmark data for [2Fe−2S] clusters with five-coordinate metal ions in their oxidized diferric state.

Experimental Section

General Considerations. All manipulations were performed under an anaerobic and anhydrous atmosphere of dinitrogen using standard Schlenk techniques or in a glovebox unless otherwise mentioned. Glassware was dried at 120 °C overnight. THF and hexane were dried over potassium benzophenone ketyl. Et_2O was dried over sodium benzophenone ketyl. MeCN, DMF, and DMSO were dried over CaH_2. KH was purchased as dispersion in mineral oil and washed with hexane prior to use. 2,6-Bis(imidazol-2-yl)pyridine[18] and $(NEt_4)_2[Fe_2S_2Cl_4]$[20] were synthesized according to literature procedures. ^{1}H NMR spectra were recorded on a Bruker Avance 500 MHz spectrometer. UV/vis spectra were recorded on a Specord S 100 spectrometer using quartz cuvettes. ESI mass spectra were recorded on a Thermo Finnigan Trace LCQ spectrometer; ESI-HRMS spectra were recorded on a Bruker FTICR APEX IV instrument. Cyclic voltammetry was performed at room temperature with a Perkin-Elmer Model 263A potentiostat/galvanostat with a glassy carbon working electrode and platinum reference and counter electrodes in DMF/$N^nBu_4PF_6$ (0.1 M). Cp^*_2Fe (added after the measurement) was used as an internal standard. Potentials were measured at a scan rate of 100 mV/s and referenced vs the $Cp^*_2Fe/Cp^*_2Fe^+$ couple and NHE ($Cp^*_2Fe/Cp^*_2Fe^+$ vs NHE: −0.23 V in DMF).[23] Mössbauer spectra were recorded at 80 K on a WissEl alternating constant acceleration spectrometer. Isomer shifts are given relative to α-iron metal at room temperature. The experimental data were fitted with Lorentzian line shapes using the MFit program (E. Bill, Max Planck Institute for Bioinorganic Chemistry, Mülheim/Ruhr, Germany).

Bis(tetraethylammonium) Bis[(2,6-bis(2-imidazolato)pyridine)-(μ-sulfido)-ferrate(III)] (1). 2,6-Bis(imidazol-2-yl)pyridine (H_2L, 425 mg, 2.0 mmol) was dissolved in THF (40 mL; stirring for 10 min was required for complete dissolution) and subsequently treated with KH (170 mg, 4.0 mmol) in one portion. After 2 h, the white suspension was diluted with MeCN (60 mL) and treated with $(NEt_4)_2[Fe_2S_2Cl_4]$ (580 mg, 1.0 mmol). The colorless solid dissolved within 2 h, while the brown product gradually precipitated from the solution within 3 h. It was separated by filtration, washed with THF (2 × 20 mL), and dried in vacuo to yield the target compound **1** (650 mg, 0.76 mmol, 76%) that was pure according to NMR and Mössbauer spectroscopy, although elemental analysis showed some inorganic impurity (most probably KCl). Recrystallization from DMF/Et_2O yielded some crystalline material suitable for X-ray diffraction but did not improve the purity of the bulk material due to gradual decomposition. ^{1}H NMR (500 MHz, MeCN-d_3): δ 1.17 (br s, 24H, NEt_4), 3.09 (br s, 16H, NEt_4), 6.90 (br s, 2H, Ar−H), 9.00 (br s, 4H, Ar−H), 12.83 (br s, 4H, Ar−H), 13.71 (br s, 4H, Ar−H). UV/vis (DMSO): λ_{max}/nm (ε/l·mol^{-1}·cm^{-1}) 310 (34000), 489 (3000). MS (ESI(+), MeCN): *m*/*z* (%) 1235 (50) $[M + 3\,NEt_4]^+$, 1105 (100) $[M + 2\,NEt_4]^+$, 985 (20) $[M + NEt_4]^+$. MS (ESI(−), MeCN): *m*/*z* (%) 724 (10) $[M - NEt_4]^-$, 595 (20) $[M - NEt_4 + H]^-$, 474 (100) $[L_2Fe]^+$. HRMS (ESI(−), MeCN) calcd (*m*/*z*) for $C_{30}H_{34}Fe_2N_{11}S_2$ $[M - NEt_4]^-$: 724.1145. Found: 724.1147.

X-Ray Crystallography. X-ray data were collected on a STOE IPDS II diffractometer (graphite monochromated Mo Kα radiation, λ = 0.71073 Å) by use of ω scans at −140 °C. The structure was solved by direct methods and refined on F^2 using all reflections with SHELX-97.[31] Hydrogen atoms were placed in calculated positions and assigned to an isotropic displacement parameter of 0.08 Å^2. Face-indexed absorption corrections were performed numerically with the program X-RED.[32] Crystal dimensions: 0.50 × 0.50 × 0.35 mm, monoclinic, space group $P2_1/c$ (No. 14), a = 11.2144(4), b = 14.4686(4), c = 13.7454(5) Å, β = 113.658(3), V = 2042.84(12) Å^3, Z = 2, F(000) = 900, ρ_{calcd} = 1.390 g cm^{-3}, μ = 0.857 mm^{-1}, T_{max}/T_{min} = 0.7269/0.6373, 1.98≤ θ ≤ 26.94°, −14 ≤ h ≤ 14, −18 ≤ k ≤ 18, −17 ≤ l ≤ 17, 26 072 data collected, 4445 unique data (R_{int} = 0.0317), 4191 data with $I > 2\sigma(I)$, 248 refined parameters, GOF (F^2) = 1.028. Final R indices: $R1$ = 0.0263 (0.0282 all data), $wR2$ = 0.0699 (0.0709 all data). Max/min residual electron density: 0.383/−0.363 e Å^{-3}.

Magnetic Measurements. Temperature-dependent magnetic susceptibilities of **1** were measured using a Quantum Design MPMS-5S SQUID magnetometer in the temperature range 295−2 K at an applied magnetic field of 0.5 T. The powdered sample was contained in a Teflon bucket and fixed in a nonmagnetic sample holder. Each raw data file for the measured magnetic moment was corrected for the diamagnetic contribution of the sample holder and the bucket. The molar susceptibilities were corrected for the diamagnetic contribution. Simulation of the experimental data with a full-matrix diagonalization of exchange coupling and Zeeman splitting was performed with the julX program (E. Bill, Max Planck Institute for Bioinorganic Chemistry, Mülheim/Ruhr, Germany) according to

$$\hat{H} = -2J\hat{S}_1\cdot\hat{S}_2 + g\mu_B(\hat{S}_1 + \hat{S}_2)B$$

Temperature-independent paramagnetism (*TIP*) and a paramagnetic impurity (*PI*) with spin S = 5/2 and Curie−Weiss behavior were included according to

$$\chi_{calc} = (1 - PI)\cdot\chi + PI\cdot\chi_{mono} + TIP$$

DFT Calculations. DFT calculations were performed using the Turbomole 5.9[33] program with the BP86 functional[27,28] or the B3LYP functional[29,30] and the def2-SV(P)[34] basis set. Calculations were based on atom coordinates of the complex dianions obtained from crystal structure data. Geometry optimizations were performed using the RELAX module. The wave function in antiferromagnetically coupled Fe/S clusters has a multideterminantal nature. In the single-determinant density functional theory (DFT), such coupling can be modeled by means of the broken-symmetry (BS) scheme, developed by Noodleman et al.[35] In this approach, either α or β spin excess is localized on the different spin centers composing the system. The resulting unrestricted wave function corresponds to a linear combination of pure spin states. Theoretical quadrupole splittings ΔE_Q were calculated from eigenvalues V of the electric field gradients according to

$$\Delta E_Q = \frac{1}{2}eQV_{zz}\cdot\left(1 + \frac{\eta^2}{3}\right)^{1/2}$$

with Q = 0.16 barn = 1.6 × 10^{-29} m^2, $\eta = (V_{xx} - V_{yy})/V_{zz}$, $|V_{xx}| < |V_{yy}| < |V_{zz}|$, 1 au = 9.72 × 10^{21} V/m^2, and 1 mm/s = 4.8075 × 10^{-8} eV. Theoretical coupling constants J for the oxidized diferric state

(31) Sheldrick, G. M. *Acta Crystallogr*. **2008**, *A 64*, 112–122.
(32) *X-RED*; STOE & CIE GmbH: Darmstadt, Germany, 2002.
(33) Ahlrichs, R.; Bär, M.; Häser, M.; Horn, H.; Kölmel, C. *Chem. Phys. Lett*. **1989**, *162*, 165–169.
(34) Weigend, F.; Ahlrichs, R. *Phys. Chem. Chem. Phys*. **2005**, *7*, 3297–3305.
(35) Noodleman, L.; Norman, J. G. *J. Chem. Phys*. **1979**, *70*, 4903–4906. Noodleman, L. *J. Chem. Phys*. **1981**, *74*, 5737–5743. Mouesca, J.-M.; Chen, J. L.; Noodleman, L.; Bashford, D.; Case, D. A. *J. Am. Chem. Soc*. **1994**, *116*, 11898. Noodleman, L.; Peng, C. Y.; Case, D. A.; Mouesca, J.-M. *Coord. Chem. Rev*. **1995**, *144*, 199–244.

were calculated from the energies of the ferromagnetic (E_{HS}) and antiferromagnetic (E_{BS}) states according to[36]

$$J = -\frac{(E_{HS} - E_{BS})}{\langle S^2\rangle_{HS} - \langle S^2\rangle_{BS}}$$

These calculations were performed on X-ray coordinates and on coordinates optimized using the antiferromagnetically coupled ground state. Illustrations of spin densities and molecular orbitals were prepared using the VMD 1.8.6[37] program and ray-traced using the POV-Ray 3.6[38] software.

(36) (a) Yamaguchi, K.; Takahara, Y.; Fueno, T. in *Applied Quantum Chemistry*; Smith, V. H., Schaefer, F., III, Morokuma, K., Eds.; D. Reidel: Boston, MA, 1986; p 155. (b) Soda, T.; Kitagawa, Y.; Onishi, T.; Takano, Y.; Shigeta, Y.; Nagao, H.; Yoshioka, Y.; Yamaguchi, K. *Chem. Phys. Lett.* **2000**, *319*, 223–230.

(37) Humphrey, W.; Dalke, A.; Schulten, K. *J. Mol. Graphics* **1996**, *14*, 33–38.

(38) Persistance of Vision Pty. Ltd. (Version 3.6), 2004, retrieved from http://www.povray.org (accessed May 2010).

Acknowledgment. We thank Steffen Meyer for synthetic support, Jörg Teichgräber for collecting the CV data, and Benjamin Schneider for additional Mössbauer measurements. Particular thanks go to one of the reviewers for his critical evaluation of the electrochemical data. Financial support by the Fonds der Chemischen Industrie (Kekulé fellowship for M.G.G.F.), the Deutsche Forschungsgemeinschaft, and the Swedish research council (International Research Training Group GRK 1422 "Metal Sites in Biomolecules: Structures, Regulation and Mechanisms"; see www.biometals.eu) is gratefully acknowledged. The investigation has also been supported by computer resources of Lunarc at Lund University.

Supporting Information Available: Experimental procedures, crystallographic data, details of SQUID measurements (Figure S1) and CV measurements (Figure S2), and details of DFT calculations (Tables S1−S3). This material is available free of charge via the Internet at http://pubs.acs.org.